Single and double In atomic layers grown on top of a single atomic $NiSi_2$ layer on Si(111)

L. V. Bondarenko,[1] A. Y. Tupchaya,[1] Y. E. Vekovshinin,[1,2] D. V. Gruznev,[1] A. N. Mihalyuk,[1,2] N. V. Denisov,[1] A. V. Matetskiy,[1] A. V. Zotov,[1] and A. A. Saranin[1]

[1]*Institute of Automation and Control Processes, FEB RAS, Vladivostok 690041, Russian Federation*

[2]*Institute of High Technologies and Advanced Materials, Far Eastern Federal University, 690950 Vladivostok, Russia*

(Received 20 May 2022; revised 27 June 2022; accepted 29 June 2022; published 15 July 2022)

Atomic sandwiches consisting of In layers with coverages ranging from ~0.5 to ~2.5 monolayers atop a single-atomic-layer $NiSi_2$ have been grown on Si(111) and have been explored using a set of experimental techniques, i.e., scanning tunneling microscopy, angle-resolved photoelectron spectroscopy, and *in situ* low-temperature transport measurements, accompanied by the density functional theory calculations. It has been found that each of the three In phases forming on the $NiSi_2$/Si(111) substrate has its definite counterpart among the In phases forming on the bare Si(111) surface. Structural, electronic, and transport properties of the single- and double-atomic In layers have been elucidated in detail.

DOI: 10.1103/PhysRevB.106.035415

I. INTRODUCTION

Metal films having a thickness of one or a few atomic layers grown on the crystalline semiconductor substrates attract considerable interest of researchers due to the abundance of structural and electronic properties. Indium-induced superstructures on Si(111) are of especial interest, in particular, due to the emergence of the superconductivity at the atomic-scale limit. The list of In/Si(111) reconstructions includes α-7 × 7, $\sqrt{3} \times \sqrt{3}$, $\sqrt{31} \times \sqrt{31}$, 4 × 1, 2 × 2, and $\sqrt{7} \times \sqrt{3}$ [1,2]. While the α-7 × 7 [3,4], $\sqrt{31} \times \sqrt{31}$ [5], and 4 × 1 [6] reconstructions are known to incorporate Si atoms in their structures, the $\sqrt{3} \times \sqrt{3}$, 2 × 2, and $\sqrt{7} \times \sqrt{3}$ reconstructions can be visualized as In films of various coverages and superstructures residing atop a bulklike terminated Si(111) substrate. Thus, the latter reconstructions can be formed via In deposition onto the Si(111)$\sqrt{3} \times \sqrt{3}$-In surface held at room temperature (RT) [7]. Understanding of the atomic arrangement and even In coverage of these reconstructions has undergone dramatic evolution during the last two decades [8–13], but even up to now complete consensus has not been reached. Nevertheless, we believe that the general self-consistent picture can be represented as follows. The $\sqrt{3} \times \sqrt{3}$-In is well established to contain 1/3 ML of In adatoms residing in the T_4 sites on Si(111). The 2 × 2-In has recently been determined to incorporate 1.0 ML of In, of which three In atoms within the 2 × 2 unit cell occupy T_4 sites, forming a trimer centered in the H_3 site, and the fourth In adatom occupies the on-top (T_1) site [14,15]. The most debated reconstructions are the $\sqrt{7} \times \sqrt{3}$-In ones [13,16–24]. It is generally accepted that there are two types of the $\sqrt{7} \times \sqrt{3}$-In structures: quasihexagonal hex-$\sqrt{7} \times \sqrt{3}$ with ~1.4 ML of In and quasirectangular rect-$\sqrt{7} \times \sqrt{3}$ with 2.4 ML of In. The hex-$\sqrt{7} \times \sqrt{3}$-In has a single-atomic-layer structure which converts upon cooling to the ground-state $\sqrt{7} \times \sqrt{7}$ structure [13,22,25,26], and the rect-$\sqrt{7} \times \sqrt{3}$-In has a double-atomic-layer structure which remains unchanged upon cooling. Regarding the electronic properties, the 2 × 2-In phase is semiconducting [14,15], the hex-$\sqrt{7} \times \sqrt{3}$-In is metallic at RT and undergoes a metal-insulator transition upon conversion to the $\sqrt{7} \times \sqrt{7}$ structure [22,23], and the rect-$\sqrt{7} \times \sqrt{3}$-In is metallic and converts into the superconductor state [27–33] at the critical temperature in the range from 1.0 to 3.2 K, depending on the evaluation technique (e.g., scanning tunneling spectroscopy [27], transport measurements [29,31], or measuring the diamagnetic response associated with the Meissner effect [32]), as well as on the sample preparation conditions, in particular, the extent of disorder in the In layer [30,33].

Bearing all these in mind, it seemed of interest to explore how the change of the substrate from the bare Si(111) to another one would affect the structure and properties of the In films. In the very recent work [34], the properties of the double-atomic-layer In film on the Si(111) covered by the single-layer Mg have been studied. In the present study, we changed the bare Si(111) substrate for the Si(111) one with a single-atomic-layer $NiSi_2$ atop. The choice of the $NiSi_2$/Si(111) template was dictated, on the one hand, by the fact that its topmost-atom structure is akin that of the bulklike terminated Si(111) substrate and, on the other hand, by the recent results where it has been shown as an advanced platform for growing exotic nano-objects, e.g., a graphenelike honeycomb lattice built of Tl atoms, thallene, [35] or a $NiSi_2$ metal sheet of atomic thickness embedded in the crystalline silicon matrix [36]. In addition, nickel silicide is an important contact material in semiconductor technology. It was found to be effective in field-effect transistors [37] and solar cells [38]. The formation of the sharp and defect-free interface with indium, which is also widely used in semiconductor technology, provides effective contact pads for technological applications. Moreover, superconductor thin films and their contacts with metals, oxides, and semiconductors are now

a focus of extensive studies for the purposes of quantum computing technologies [39–42]. The search for new combinations with suppressed defect-associated decoherence noise is an important task in this field [43].

In the present study, atomic sandwiches consisting of In layers with coverages ranging from ∼0.5 to ∼2.5 ML atop single-atomic-layer $NiSi_2$ have been grown on Si(111) and their structural, electronic, and transport properties have been explored using a set of experimental techniques, i.e., scanning tunneling microscopy (STM), low-energy electron diffraction (LEED), angle-resolved photoelectron spectroscopy (ARPES), and *in situ* transport measurements, accompanied by density functional theory (DFT) calculations. The obtained results are compared with those for the counterpart In films grown on a bare Si(111) surface.

II. EXPERIMENTAL AND CALCULATION DETAILS

The STM, LEED, and ARPES experiments were performed in an ultrahigh-vacuum Omicron MULTIPROBE system with a base pressure better than 2.0×10^{-10} Torr. Atomically clean Si(111)7×7 surfaces were prepared *in situ* by flashing to 1280 °C after the samples were first outgassed at 600 °C for several hours. The In was deposited from a tantalum tube and the Ni from an electron beam evaporator. STM images were acquired using Omicron variable-temperature STM-XA operating in a constant-current mode. Mechanically cut PtIr tips were used as STM probes after annealing in vacuum. ARPES measurements were conducted using a VG Scienta R3000 electron analyzer and high-flux He discharge lamp ($h\nu = 21.2$ eV) with a toroidal-grating monochromator as a light source. Transport measurements were conducted in the UNISOKU USM 1500 LT system, equipped with a superconducting magnet and four-point-probe (4PP) technique, which provides the lowest temperature of ∼2 K.

The DFT calculations were performed using the Vienna Ab initio Simulation Package (VASP) [44,45], with core electrons represented by projector augmented wave (PAW) potentials [46,47]. To get an accurate Si band gap, we applied the DFT-1/2 self-energy correction method [48]. Spin-orbit interaction (SOI) was included in all the types of calculations. The Si(111)1×1-(In, Ni) cell geometry was simulated by a repeating slab of 10 Si bilayers and a vacuum region of ∼15 Å. Si atoms in the bottom three bilayers were fixed at their bulk positions, the top seven bilayers were allowed to fully relax, and dangling bonds on the bottom surface were saturated by hydrogen atoms. Γ-centered 12 × 12 × 1 *k*-point mesh was used. The geometry optimization was performed until the residual force was smaller than 10 meV/Å.

III. RESULTS AND DISCUSSION

To form the $In/NiSi_2/Si(111)$ atomic sandwiches, we employed the technique used before for fabrication of the parent $Tl/NiSi_2/Si(111)$ [49] and $Pb/NiSi_2/Si(111)$ [50] sandwiches. According to this technique, the metal atomic layer of Tl, Pb, or In is grown first on the bare Si(111) surface, then 1.0 ML of Ni is deposited onto the metal layer, followed by sample annealing to 300 °C, which results in Ni intercalation into the top Si(111) bilayer and the formation of the single-layer $NiSi_2$ sandwiched between a metal capping layer and a Si(111) substrate.

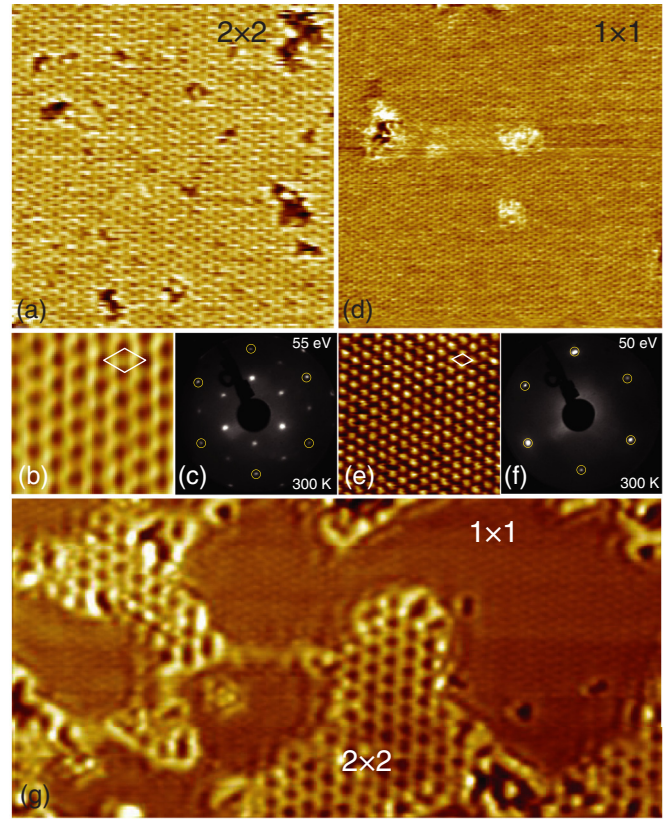

FIG. 1. (a) Large-scale (25 × 25 nm^2) and (b) high-resolution (5.0 × 5.0 nm^2) STM images and (c) LEED pattern of the In/Si(111)2×2 surface. (d) Large-scale (25 × 25 nm^2) and (e) high-resolution (5.0 × 5.0nm^2) STM images and (f) LEED pattern of the $In/NiSi_2/Si(111)1 \times 1$ surface formed by intercalation of 1.0 ML of Ni into the In/Si(111)2×2 sample. The main reflections in (c) and (f) are marked by yellow circles. (g) 26 × 13 nm^2 filled-state (−0.8 eV) STM image from the surface obtained by intercalation of ∼0.6 ML Ni into the In/Si(111)2 × 2, that results in the coexistence of the 2 × 2-In and 1 × 1-In domains residing on bare Si(111) and $NiSi_2/Si(111)$, respectively. The STM bias voltages used were (a) −1.0 V, (b) +0.01 V, (d) −0.01 V, (e) −0.01 V, and (g) −0.8 V.

In the present study, the 2 × 2-In layer with 1.0 ML of In [Figs. 1(a)–1(c)] was used as a starting point for fabrication of most of the $In/NiSi_2/Si(111)$ sandwiches. In particular, when 1.0 ML of Ni is intercalated beneath the 2 × 2-In, the structure of the In layer changes from 2 × 2 to 1 × 1 [Figs. 1(d)–1(f)]. When less than 1.0 ML of Ni is deposited, patches of the 2 × 2-In (having a characteristic honeycomblike STM appearance [14]) atop a bare Si(111) coexist with regions of the 1 × 1-In atop $NiSi_2/Si(111)$ [Fig. 1(g)]. The structure of the 1 × 1-In layer has been elucidated to be very similar to that of the 1 × 1-Tl layer at the $NiSi_2/Si(111)1 \times 1$ surface, where metal adatoms occupy the T_4 sites [49] (Fig. 2(a); like those in the Tl/Si(111) system [51,52]). As a result, the electronic band structures of the $In/NiSi_2/Si(111)1 \times 1$ and $Tl/NiSi_2/Si(111)1 \times 1$ systems are almost identical, as revealed in the ARPES observations [Figs. 2(b) and 2(c)]. For comparison of the ARPES data and DFT calculation results

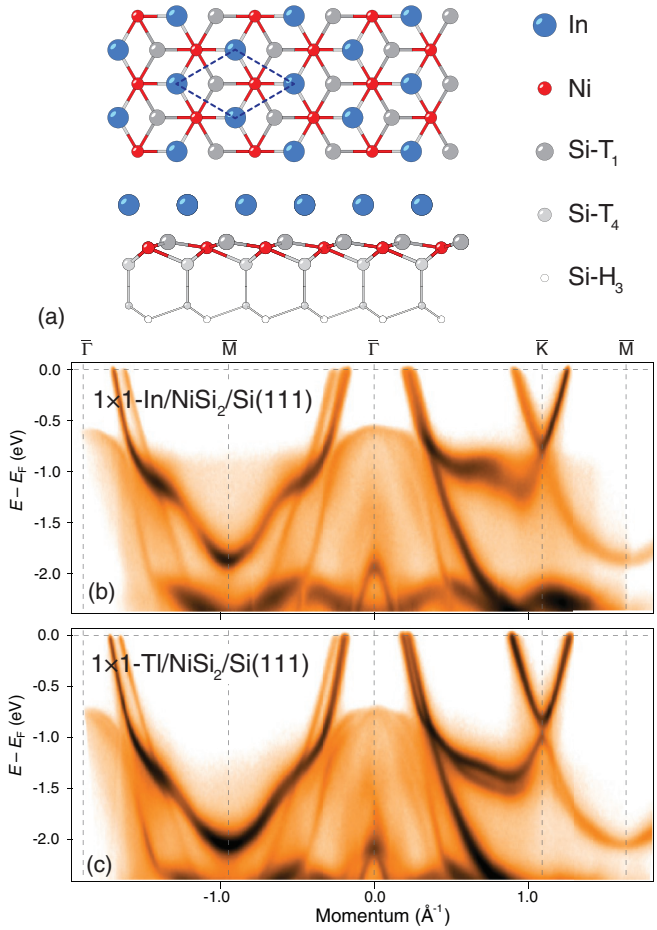

FIG. 2. (a) Ball-and-stick model of the $In/NiSi_2/Si(111)1 \times 1$ phase with 1.0 ML of In. The In atoms are shown by blue balls, Ni atoms by red balls, and Si atoms by gray balls, having various sizes and contrast depending on the atomic layer. (b) ARPES spectrum from the $In/NiSi_2/Si(111)1 \times 1$ surface shown in comparison with (c) that from the $Tl/NiSi_2/Si(111)1 \times 1$ surface. Both surfaces contain the same coverage of 1.0 ML of adsorbate, In and Tl, respectively. ARPES spectra were recorded at 78 K.

for the $In/NiSi_2/Si(111)1 \times 1$ and $Tl/NiSi_2/Si(111)1 \times 1$ systems with 1.0 ML of In and Tl, respectively, see the Supplemental Material [53].

However, a certain difference in their properties does exist. In the case of the $Tl/NiSi_2/Si(111)$ system, if the Tl layer containing ~2/3 ML is cooled to temperatures below ~150 K, it converts to a $\sqrt{3} \times \sqrt{3}$ superstructure with a honeycomb graphenelike geometry, due to the ordering of the vacancies [35]. In the case of the 1×1-In layer with ~2/3 ML of In on $NiSi_2/Si(111)$ [which is formed when the $\sqrt{3} \times \sqrt{3}$-In (1/3 ML of In) and 2×2-In (1.0 ML of In) domains occupy equal areas at the initial In/Si(111) surface], upon cooling to the low temperatures, vacancies become frozen in the random positions without the formation of any ordered superstructure.

With increasing In coverage beyond 1.0 ML, a new phase, having a greater apparent STM height, starts to form and covers the entire surface at total In coverage of ~1.5 ML (Figs. 3). Hence, it can be thought to have hex-$\sqrt{7} \times \sqrt{3}$-In as a parent

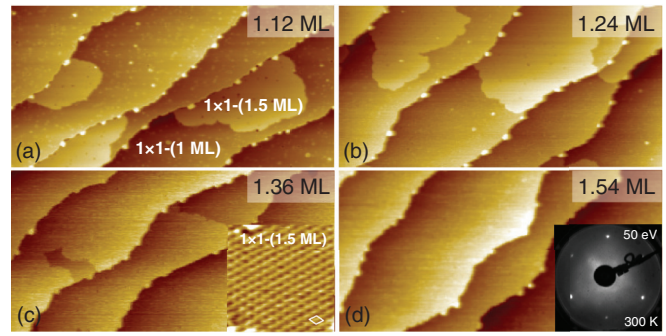

FIG. 3. Set of large-scale (a-d) (400×200 nm^2) RT-STM images illustrating the development of the new phase in the $In/NiSi_2/Si(111)$ system with increasing In coverage beyond 1.0 ML, until it covers the whole surface at ~1.5 ML of In. Insets in (c) and (d) show the high-resolution (5×5 nm^2) RT-STM image and LEED pattern, respectively, which indicate that the new phase has a 1×1 periodicity. All STM images were recorded at −1.0 V bias voltage, except for that in the inset in (c) recorded at +0.01 V.

counterpart among In layers on the bare Si(111) surface. At RT, the phase displays a 1×1 structure both in STM and LEED [see insets in Figs. 3(c) and 3(d), respectively] and will be referred to hereafter as 1×1-In (1.5 ML) in order to distinguish it from the previous 1×1-In (1.0 ML).

Upon cooling to liquid-nitrogen temperatures (e.g., 80 to 110 K), the structure of the 1×1-In (1.5 ML) phase undergoes a dramatic change. In the large-scale low-temperature (LT)-STM images, the surface structure might look, at a glance, as akin to the hex-$\sqrt{7} \times \sqrt{3}$-In surface, having a similar striped structure with stripes running along the $\sqrt{3}$ (i.e., $[\bar{1}01]$) directions [Fig. 4(a)]. However, the high-resolution STM images [Fig. 4(b)] and, especially, the LT-LEED pattern [Fig. 4(c)] clearly show that the surface has its own specific periodicity, which was elucidated to be $2\sqrt{19} \times 2\sqrt{3}$ [i.e., $\begin{pmatrix} 6 & -4 \\ 2 & 4 \end{pmatrix}$ in matrix notation]. Figure 4(e) illustrates the relation between the real-space $2\sqrt{19} \times 2\sqrt{3}$ and $\sqrt{7} \times \sqrt{3}$ lattices, shown in pink and blue, respectively. Figure 4(d) shows the schematic LEED (reciprocal lattice) built for the $2\sqrt{19} \times 2\sqrt{3}$ lattice. Comparing the LEED schematics with the experimental LEED pattern [Fig. 4(c)], one can see a clear correspondence, though some of the reflections are missing in the experimental LEED pattern. This can be attributed to the particular form factors of this long-periodic structure, as well as to an incomplete long-range ordering of the surface, which can already be noticed in the high-resolution STM image in Fig. 4(b).

When In coverage is increased further, the next phase starts to develop [Fig. 5(a)]. It covers the entire surface at total In coverage of ~2.5 ML [Fig. 5(b)], and therefore it can be thought to have a relation to the double-layer rect-$\sqrt{7} \times \sqrt{3}$-In phase. Indeed, the $In/NiSi_2/Si(111)$ phase with ~2.5 ML of In displays the $\sqrt{7} \times \sqrt{3}$ periodicity, well resolved both in the high-resolution STM images [Fig. 5(c)] and LEED patterns [Figs. 5(d) and 5(e)]. The same periodicity and even certain similarity in the surface structures are especially apparent, when rect-$\sqrt{7} \times \sqrt{3}$-In phases on the $NiSi_2/Si(111)$ and bare Si(111) surfaces coexist, as in Fig. 5(c), showing the

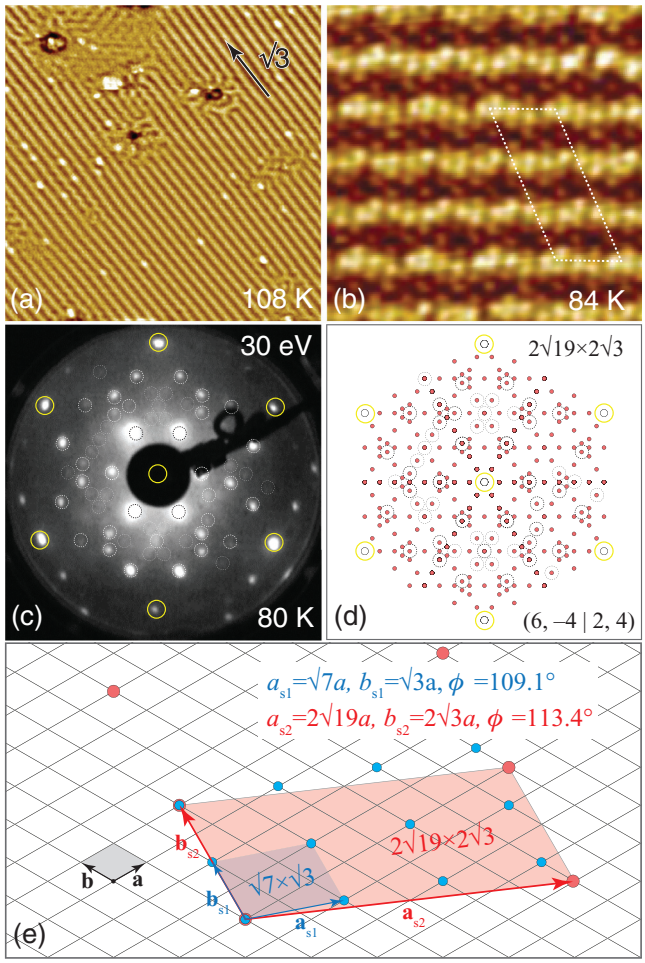

FIG. 4. (a) Large-scale (30 × 30 nm^2) empty-state (+1.5 V) and (b) high-resolution (6 × 6 nm^2) empty-state (+1.0 V) STM images and (c) LEED pattern from the In/$NiSi_2$/Si(111) surface with ∼1.5 ML of In cooled to 80 K. (d) Schematic LEED pattern (reciprocal lattice) from the $2\sqrt{19} \times 2\sqrt{3}$ lattice. The reflections having counterparts in the experimental LEED pattern are outlined with the dashed circles. (e) Schematics illustrating the relation between the $2\sqrt{19} \times 2\sqrt{3}$ and $\sqrt{7} \times \sqrt{3}$ lattices in the real space, shown in pink and blue, respectively.

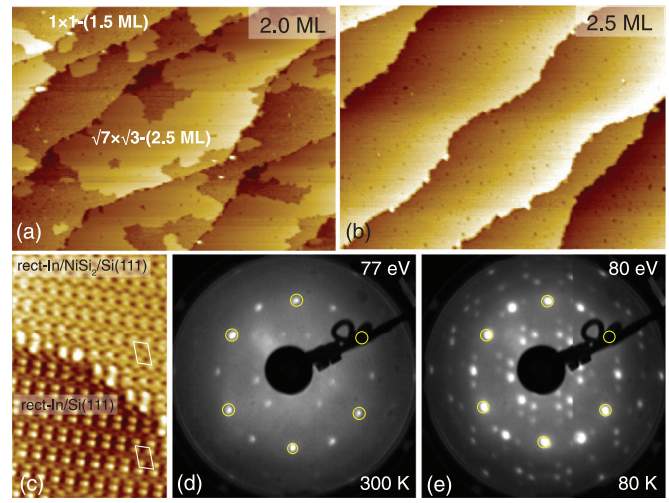

FIG. 5. Large-scale (400 × 300 nm^2) filled-state (−1.0 V) STM images of the In/$NiSi_2$/Si(111) surface with total In coverage of (a) ∼2.0 and (b) ∼2.5 ML. (c) High-resolution (6.5 × 10 nm^2) empty-state (+0.5 V) STM image, where the region of the rect-$\sqrt{7} \times \sqrt{3}$-In phase residing on the bare Si(111) surface (lower part of the image) coexists with that of the rect-$\sqrt{7} \times \sqrt{3}$-In phase formed atop the $NiSi_2$/Si(111) surface (upper part of the image). LEED patterns from the rect-$\sqrt{7} \times \sqrt{3}$-In phase formed atop the $NiSi_2$/Si(111) surface recorded at (d) RT and (e) 80 K. The main reflections in the LEED patterns are outlined by the yellow circles to guide the eye.

STM image from the surface with an incomplete $NiSi_2$ layer. In addition, like the bare rect-$\sqrt{7} \times \sqrt{3}$-In phase, the rect-$\sqrt{7} \times \sqrt{3}$-In phase on $NiSi_2$ does not undergo any structural changes upon cooling, except improved ordering, as reflected by the increased brightness of the $\sqrt{7} \times \sqrt{3}$ LEED pattern recorded at 80 K [Fig. 5(e)].

Tentative structural model of the rect-$\sqrt{7} \times \sqrt{3}$-In phase on $NiSi_2$/Si(111) is shown in Fig. 6(b). It is essentially a double-layer rect-$\sqrt{7} \times \sqrt{3}$-In model structure [Fig. 6(a)] [11], which was placed atop a single-layer $NiSi_2$ on Si(111) and was allowed to relax. Relaxation mostly affects the first In layer adjacent to the $NiSi_2$/Si(111) surface, making it become slightly distorted. Meanwhile, the outer In layer has an almost ideal rectangular structure similar to that in the rect-$\sqrt{7} \times \sqrt{3}$-In phase on the bare Si(111) surface [11,21]. Simulated STM images for the rect-$\sqrt{7} \times \sqrt{3}$-In phase on $NiSi_2$/Si(111) demonstrate a clear correspondence to their experimental counterparts [Fig. 6(c)], which sounds supportive for the proposed structural model.

Figure 7 shows electronic band structures calculated in the $\sqrt{7} \times \sqrt{3}$ surface Brillouin zone (SBZ) for the double-layer rect-$\sqrt{7} \times \sqrt{3}$-In structures placed on the bare Si(111) surface and on the single-layer $NiSi_2$ on Si(111). In particular, the calculated band structure for the rect-$\sqrt{7} \times \sqrt{3}$-In on Si(111) [Fig. 7(a)] with a set of metallic bands responsible for the properties of the nearly free electron metal in the two dimensions appears to be in proper agreement with the previously reported ARPES data [54] and calculation results [11]. The addition of the $NiSi_2$ interlayer to the In/Si(111) system results in the appearance of the two surplus holelike bands centered in the $\overline{\Gamma}$ point. Their hybridization with the original In-associated bands (in particular, due to the anticrossing) modifies the electronic band structure of the system. For detailed element-projected band structures of In-rect/Si(111) and In-rect/$NiSi_2$/Si(111) systems, see Fig. 2S in the Supplemental Material [53].

Let us now consider the transport properties of the In/$NiSi_2$/Si(111) systems, starting with those with the single-atomic In layers, 1 × 1-In and $2\sqrt{19} \times 2\sqrt{3}$-In (Fig. 8). In particular, Figure 8(a) shows the temperature dependencies of the sheet resistance of the 1×1-In in the absence of the magnetic field (brown curve) and with magnetic field of 1.0 T applied perpendicular to the sample (green curve). At low temperatures, the system has a sheet resistance of the order of ∼555 Ohm/sq and displays a basic metallic type of conductivity that stems from the occurrence of the three metallic bands, two hole bands centered in the $\overline{\Gamma}$ point, and one electron band with pockets in the $\overline{K}$ points [Fig. 2(b)]. A slight increase

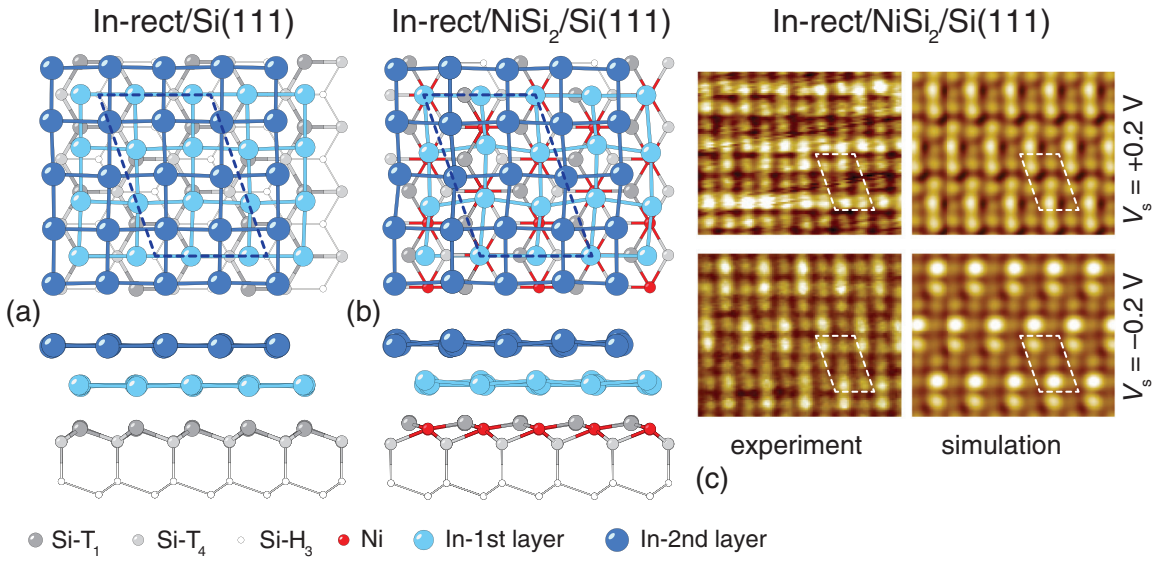

FIG. 6. Ball-and-stick models of the double-layer rect-$\sqrt{7} \times \sqrt{3}$-In structure placed (a) on the bare Si(111) surface and (b) on the single-layer $NiSi_2$ on Si(111). The In atoms of the first and second layers are shown by dark and light blue balls, respectively, the Ni atoms by red balls, and the Si atoms by gray balls having various sizes and contrast, depending on the atomic layer. (c) Comparison of the dual-polarity (± 0.2 eV) experimental (left column) and simulated (right column) STM images of the double-layer rect-$\sqrt{7} \times \sqrt{3}$-In structure placed on a single-layer $NiSi_2$ on Si(111).

in the resistance when going below ~15 K is a sign of the quantum corrections. The increase is logarithmic in temperature, as expected for a two-dimensional (2D) case. One can see that the resistance increases with applied magnetic field, indicating the weak antilocalization (WAL) effect [55].

The $2\sqrt{19} \times 2\sqrt{3}$-In layer expectedly demonstrates stronger metallic properties in comparison with those of the 1×1-In layer, since it has a greater density of the metal atoms in the In layer. The sample has a significantly lower resistance of the order ~150 Ohm/sq, which is almost linear in temperature [Fig. 8(b)], and which corresponds to the effect of strong electron-electron interaction. In this system, the contribution of the WAL effect, which shows up in the increase of the resistance in the magnetic field, appears to be less sufficient compared to the effect produced by the electron-electron interaction.

Transport properties of the double-layer rect-$\sqrt{7} \times \sqrt{3}$-In phase seem to be of especial interest due to the occurrence of the 2D superconductivity. In the present experiments, we conducted low-temperature sheet-resistance $R_s(T)$ measurements for both possible environments of the rect-$\sqrt{7} \times \sqrt{3}$-In phase, i.e., those with rect-$\sqrt{7} \times \sqrt{3}$-In on the bare Si(111) and Si(111) covered by a single-layer $NiSi_2$ sheet (Fig. 9). In general agreement with the previously reported data [29,31,33], the rect-$\sqrt{7} \times \sqrt{3}$/Si(111) sample displays the normal-phase sheet resistance R_n of ~50 Ohm/sq and transition into the superconducting state at a critical temperature $T_c \sim 2.9$ K (red curves in Fig. 9). The critical temperature was determined at a level of 50% of the resistance in the normal state on a plateau above the temperature of

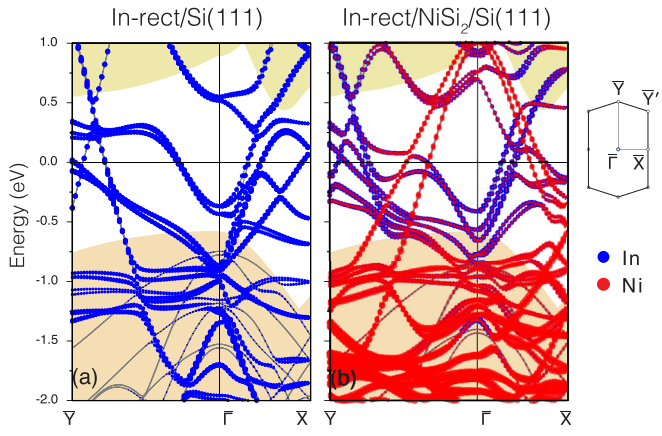

FIG. 7. Electronic band structures calculated in the $\sqrt{7} \times \sqrt{3}$ SBZ for the double-layer rect-$\sqrt{7} \times \sqrt{3}$-In structures placed (a) on the bare Si(111) surface and (b) on the single-layer $NiSi_2$ on Si(111). Orbitals associated with In and Ni are indicated in blue and red, respectively. Shaded regions indicate projected Si bulk bands.

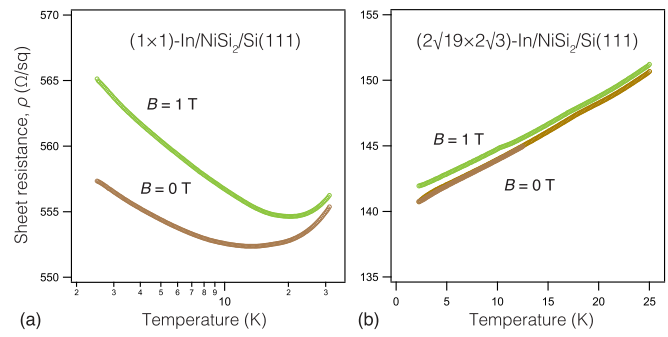

FIG. 8. Temperature dependencies of the sheet resistance of the single-atomic-layer In films on the $NiSi_2$/Si(111) substrate, (a) 1×1-In and (b) $2\sqrt{19} \times 2\sqrt{3}$-In, in the absence of the magnetic field (brown curves) and with magnetic field of 1.0 T applied perpendicular to the sample (green curve).

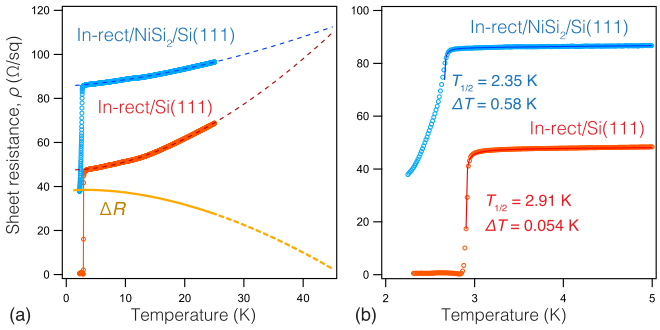

FIG. 9. Comparison of the transport properties of the double-layer rect-$\sqrt{7} \times \sqrt{3}$ phase on the bare Si(111) (red curves) and Si(111) covered by a single-layer $NiSi_2$ sheet (blue curves) in the temperature ranges of (a) 2.3 to 45 K and (b) 2.3 to 5.0 K. The dashed red and blue curves in (a) represent the extrapolation of the experimental dependencies to the higher temperatures, as a sum of three terms, constant due to the residual resistance, linear dependence due to the electron-electron interaction, and power-law dependence due to the electron-phonon interaction. The yellow curve in (a) shows the resistance difference for the rect-$\sqrt{7} \times \sqrt{3}/NiSi_2/Si(111)$ and rect-$\sqrt{7} \times \sqrt{3}/Si(111)$ samples.

the superconducting transition. The normal-phase resistance of the rect-$\sqrt{7} \times \sqrt{3}/NiSi_2/Si(111)$ sample (blue curves in Fig. 9) is about twice greater, while the critical temperature shifts to the lower temperature, ~2.4 K. The shapes of the $R_s(T)$ dependencies near the transition temperature for the two samples have also noticeable qualitative differences, as illustrated in Fig. 9(b). In particular, while the resistivity drop for the rect-$\sqrt{7} \times \sqrt{3}/Si(111)$ sample is steep, in the case of the rect-$\sqrt{7} \times \sqrt{3}/NiSi_2/Si(111)$ sample, it is apparently more sloping. Namely, the transition width determined using the "10-90" criterion as $\Delta T_c = T_1(0.9R_n) - T_1(0.1R_n)$ is 0.054 and 0.58 K for the rect-$\sqrt{7} \times \sqrt{3}/Si(111)$ and rect-$\sqrt{7} \times \sqrt{3}/NiSi_2/Si(111)$ samples, respectively. Note that for the rect-$\sqrt{7} \times \sqrt{3}/NiSi_2/Si(111)$ sample, the $T_1(0.1R_n)$ was estimated through extrapolation of the experimental dependence to the lower temperatures.

Lowered critical temperature and increased transition width are the typical signs of the presence of the magnetic impurities in the metallic film [56,57]. Nickel is the only magnetic element present in the rect-$\sqrt{7} \times \sqrt{3}/NiSi_2/Si(111)$ sample. However, the occurrence of its magnetic properties depends on its chemical environment. The $NiSi_2$ is known to be a nonmagnetic material in the bulk form [58]. The present DFT analysis also does not reveal any indication of magnetism for the rect-$\sqrt{7} \times \sqrt{3}/NiSi_2/Si(111)$ system. However, there are a number of InNi alloys possessing magnetic properties [59]. Thus, it can be suggested that some of the Ni atoms from the $NiSi_2$ atomic layer might dissolve into the rect-$\sqrt{7} \times \sqrt{3}$-In double layer and act as magnetic impurities. Note that concentration of the magnetic Ni atoms might be quite small, as the effect of the decrease of the critical temperature $\delta T/T_{c0}$ is of the order of $-c\varepsilon_F/k_BT_K$, where c is the concentration of the magnetic impurity, ε_F is the Fermi energy, T_K is the Kondo temperature, and k_B is the Boltzmann constant [56]. The value of $\varepsilon_F/k_BT_K \gg 1$, as the Fermi energy is about 6.9 eV for the rect-$\sqrt{7} \times \sqrt{3}$ [54], while the Kondo temperature is of the order of 100 K, as we can see later.

The yellow curve in Fig. 9(a) shows the difference between the sheet-resistance temperature dependencies of the rect-$\sqrt{7} \times \sqrt{3}$ on the $NiSi_2$ and Si(111) surfaces, ΔR. The saturation of ΔR towards zero temperature suggests the presence of the Kondo effect. For the quantitative estimation of the Kondo parameters, we follow the results of [60], which show that the scaled resistivity $R_K(T)/R_K(0)$ follows almost identical universal functions of T/T_K. As a possible way to estimate the Kondo temperature, we used the Anderson model for the low-temperature Fermi-liquid regime [61], which yields the lower limit for the Kondo temperature of $T_K \approx 115$ K.

IV. CONCLUSIONS

In conclusion, we have grown single- and double-atomic-layer In films atop a single-layer $NiSi_2$ on Si(111) and explored their structural, electronic, and transport properties using a set of experimental techniques, including LEED, STM, ARPES, and low-temperature 4PP conductivity measurements, in conjunction with the DFT calculations. It has been found that each of the three In phases forming on the $NiSi_2/Si(111)$ substrate has its definite counterpart among the In phases forming on the bare Si(111) surface. In particular, the single-atomic-layer 2×2-In structure with 1.0 ML of In on Si(111) can serve as a counterpart for the 1×1-In phase grown on $NiSi_2/Si(111)$, which also adopts 1.0 ML of In, but has a different structure which appears to be similar to that of the Tl atomic layer on Si(111). In turn, the other single-atomic-layer In phase on Si(111), namely, hex-$\sqrt{7} \times \sqrt{3}$-In having ~1.4 ML In coverage, can be considered as a counterpart for the In layer forming on $NiSi_2/Si(111)$ at ~1.5 ML of In. At RT, this layer displays, in LEED and STM observations, a 1×1 structure, which converts upon cooling to the striped structure having the $2\sqrt{19} \times 2\sqrt{3}$ periodicity. The double-atomic-layer In film grown on $NiSi_2/Si(111)$ at ~2.5 ML of In appears to be structurally akin to the double-atomic-layer rect-$\sqrt{7} \times \sqrt{3}$-In phase forming on the bare Si(111) substrate. Like the rect-$\sqrt{7} \times \sqrt{3}$-In phase, it also demonstrates superconducting properties, albeit less advanced. A side effect of the double-atomic-layer In phase formation on $NiSi_2/Si(111)$ resides in the plausible dissolution of small amounts of Ni into the In layer, where Ni atoms due to the In environment become magnetic. The presence of magnetic impurities results in the shift of the superconducting critical temperature towards the lower temperatures and increased transition width.

ACKNOWLEDGMENTS

This work was supported by the Russian Science Foundation (Grant No. 19-12-00101) [62]. The part of the work on the STM observations was partially supported by the Russian Foundation for Basic Research Grant No. 20-02-00510. The calculations were conducted using the equipment of Shared Resource Center "Far Eastern Computing Resource" IACP FEB RAS [63].

[1] H. Hirayama, S. Baba, and A. Kinbara, Electron energy loss measurements of In/Si(111) superstructures: Correlation of the spectra with surface superstructures, Appl. Surf. Sci. **33-34**, 193 (1988).

[2] J. Kraft, M. G. Ramsey, and F. P. Netzer, Surface reconstructions of In on Si(111), Phys. Rev. B **55**, 5384 (1997).

[3] J. L. Li, J. F. Jia, X. J. Liang, X. Liu, J. Z. Wang, Q. K. Xue, Z. Q. Li, J. S. Tse, Z. Zhang, and S. B. Zhang, Spontaneous Assembly of Perfectly Ordered Identical-Size Nanocluster Arrays, Phys. Rev. Lett. **88**, 066101 (2002).

[4] J. H. Byun, J. S. Shin, P. G. Kang, H. Jeong, and H. W. Yeom, Formation and electronic states of in nanoclusters on the Si(111)-7 × 7 surface, Phys. Rev. B **79**, 235319 (2009).

[5] E. N. Chukurov, A. A. Alekseev, V. G. Kotlyar, D. A. Olyanich, A. V. Zotov, and A. A. Saranin, First-principles study of Si(111)$\sqrt{31}\times\sqrt{31}$-In reconstruction, Surf. Sci. **606**, 1914 (2012).

[6] O. Bunk, G. Falkenberg, J. H. Zeysing, L. Lottermoser, R. L. Johnson, M. Nielsen, F. Berg-Rasmussen, J. Baker, and R. Feidenhans'l, Structure determination of the indium-induced Si(111)-(4×1) reconstruction by surface X-ray diffraction, Phys. Rev. B **59**, 12228 (1999).

[7] A. A. Saranin, A. V. Zotov, T. Numata, O. Kubo, K. V. Ignatovich, V. G. Lifshits, M. Katayama, and K. Oura, Structural transformations at room temperature adsorption of in on Si(111)$\sqrt{3}\times\sqrt{3}$–In surface: LEED–AES–STM study, Surf. Sci. **388**, 299 (1997).

[8] S. L. Surnev, J. Kraft, and F. P. Netzer, Modification of overlayer growth kinetics by surface interlayers: The Si(111)$\sqrt{7}\times\sqrt{3}$−indium surface, J. Vac. Sci. Technol. A **13**, 1389 (1995).

[9] J. Kraft, S. L. Surnev, and F. P. Netzer, The structure of the indium–Si(111) ($\sqrt{7}\times\sqrt{3}$) monolayer surface, Surf. Sci. **340**, 36 (1995).

[10] J. Kraft, M. G. Ramsey, and F. P. Netzer, Strain relief, close-packed overlayer formation and discommensurate phases: In on Si(111), Surf. Sci. **372**, L271 (1997).

[11] J. W. Park and M. H. Kang, Double-Layer In Structural Model for the In/Si(111)-$\sqrt{7}\times\sqrt{3}$ Surface, Phys. Rev. Lett. **109**, 166102 (2012).

[12] J. W. Park and M. H. Kang, Hexagonal indium double layer on Si(111)-$\sqrt{7}\times\sqrt{3}$, Phys. Rev. B **92**, 045306 (2015).

[13] J. W. Park and M. H. Kang, Single-Layer Limit of Metallic Indium Overlayers on Si(111), Phys. Rev. Lett. **117**, 116102 (2016).

[14] J. P. Chou, C. M. Wei, Y. L. Wang, D. V. Gruznev, L. V. Bondarenko, A. V. Matetskiy, A. Y. Tupchaya, A. V. Zotov, and A. A. Saranin, Atomic structure and electronic properties of the In/Si(111)2×2 surface, Phys. Rev. B **89**, 155310 (2014).

[15] S. G. Kwon and M. H. Kang, Honeycomb network of indium trimers and monomers on Si(111)-(2×2), Phys. Rev. B **89**, 165304 (2014).

[16] D. Shin, J. Woo, Y. Jean, H. Shim, and G. Lee, Investigation of $\sqrt{7}\times\sqrt{3}$ structures grown on In/Si(111) surfaces at room temperature, J. Korean Phys. Soc. **67**, 1192 (2015).

[17] B. Shang, L. F. Yan, and J. I. Yang, First-principles study of geometric and electronic structures of Si(111)-$\sqrt{7}\times\sqrt{3}$-In surface reconstruction, Chin. J. Chem. Phys. **25**, 403 (2012).

[18] K. Uchida and A. Oshiyama, Identification of metallic phases of In atomic layers on Si(111) surfaces, Phys. Rev. B **87**, 165433 (2013).

[19] M. Skiścim, S. Bilińska, K. Idczak, and L. Markowski, Low coverage Si(111)$\sqrt{7}\times\sqrt{3}$-In reconstruction: Deposition rate effect, Appl. Surf. Sci. **304**, 103 (2014).

[20] T. Suzuki, J. Lawrence, M. Walker, J. M. Morbec, P. Blowey, K. Yagyu, P. Kratzer, and G. Costantini, Indium coverage of the Si(111)-$\sqrt{7}\times\sqrt{3}$-In surface, Phys. Rev. B **96**, 035412 (2017).

[21] T. Shirasawa, S. Yoshizawa, T. Takahashi, and T. Uchihashi, Structure determination of the Si(111)-$\sqrt{7}\times\sqrt{3}$-In atomic-layer superconductor, Phys. Rev. B **99**, 100502(R) (2019).

[22] S. Terakawa, S. Hatta, H. Okuyama, and T. Aruga, Structure and phase transition of a uniaxially incommensurate In monolayer on Si(111), Phys. Rev. B **100**, 115428 (2019).

[23] S. Terakawa, S. Hatta, H. Okuyama, and T. Aruga, Identification of single-layer metallic structure of indium on Si(111), J. Phys.: Condens. Matter **30**, 365002 (2018).

[24] J. Woo, H. Shim, and G. Lee, $\sqrt{7}\times\sqrt{3}$ surface with a double layer of In on Si(111) exhibiting both hexagonal and rectangular features, J. Phys.: Condens. Matter **31**, 465001 (2019).

[25] A. A. Saranin, A. V. Zotov, M. Kishida, Y. Murata, S. Honda, M. Katayama, K. Oura, D. V. Gruznev, A. Visikovskiy, and H. Tochihara, Reversible phase transitions in the pseudomorphic $\sqrt{7}\times\sqrt{3}$-hex In layer on Si(111), Phys. Rev. B **74**, 035436 (2006).

[26] A. N. Mihalyuk, A. A. Alekseev, C. R. Hsing, C. M. Wei, D. V. Gruznev, L. V. Bondarenko, A. V. Matetsliy, A. Y. Tupchaya, A. V. Zotov, and A. A. Saranin, Low-temperature one-atom-layer $\sqrt{7}\times\sqrt{7}$-In phase on Si(111), Surf. Sci. **649**, 14 (2016).

[27] T. Zhang, P. Cheng, W. J. Li, Y. J. Sun, G. Wang, X. G. Zhu, K. He, L. Wang, X. Ma, X. Chen, Y. Wang, Y. Liu, H. Q. Lin, J. F. Jia, and Q. K. Xue, Superconductivity in one-atomic-layer metal films grown on Si(111), Nat. Phys. **6**, 104 (2010).

[28] T. Uchihashi, P. Mishra, M. Aono, and T. Nakayama, Macroscopic Superconducting Current through a Silicon Surface Reconstruction with Indium Adatoms: Si(111)-($\sqrt{7}\times\sqrt{3}$)-In, Phys. Rev. Lett. **107**, 207001 (2011).

[29] M. Yamada, T. Hirahara, and S. Hasegawa, Magnetoresistance Measurements of a Superconducting Surface State of In-Induced and Pb-Induced Structures on Si(111), Phys. Rev. Lett. **110**, 237001 (2013).

[30] S. Yoshizawa, H. Kim, Y. Hasegawa, and T. Uchihashi, Disorder-induced suppression of superconductivity in the Si(111)-($\sqrt{7}\times\sqrt{3}$)-In surface: Scanning tunneling microscopy study, Phys. Rev. B **92**, 041410(R) (2015).

[31] S. Yoshizawa, T. Kobayashi, Y. Nakata, K. Yaji, K. Yokota, F. Komori, S. Shin, K. Sakamoto, and T. Uchihashi, Atomic-layer Rashba-type superconductor protected by dynamic spin-momentum locking, Nat. Commun. **12**, 1462 (2021).

[32] Y. Wu, M. C. Duan, N. Liu, G. Yao, D. Guan, S. Wang, Y. Y. Li, H. Zheng, C. Liu, and J. F. Jia, Diamagnetic response of a superconducting surface superstructure: Si(111)-$\sqrt{7}\times\sqrt{3}$-In, Phys. Rev. B **99**, 140506(R) (2019).

[33] Y. Wu, G. Yao, Y. Qu, X. Wang, N. Liu, M. C. Duan, D. D. Guan, S. Wang, H. Zheng, Y. Y. Li, C. Liu, and J. F. Jia, Influence of disorder on superconductivity in the Si(111)-$\sqrt{7}\times\sqrt{3}$-In surface, Appl. Phys. Lett. **117**, 172601 (2020).

[34] S. Terakawa, S. Hatta, H. Okuyama, and T. Aruga, Ultrathin (In, Mg) films on Si(111): A nearly freestanding double-layer metal, Phys. Rev. B **105**, 125402 (2022).

[35] D. V. Gruznev, L. V. Bondarenko, A. Y. Tupchaya, A. N. Mihalyuk, S. V. Eremeev, A. V. Zotov, and A. A. Saranin,

Thallene: Graphene-like honeycomb lattice of Tl atoms frozen on single-layer $NiSi_2$, 2D Mater. **7**, 045026 (2020).

[36] L. V. Bondarenko, A. Y. Tupchaya, Y. E. Vekovshinin, D. V. Gruznev, A. N. Mihalyuk, D. A. Olyanich, Y. P. Ivanov, A. V. Matetskiy, A. V. Zotov, and A. A. Saranin, Metal sheet of atomic thickness embedded in silicon, ACS Nano **15**, 19357 (2021).

[37] F. Fuchs, S. Gemming, and J. Schuster, Electron transport through NiS_2-Si contacts and their role in reconfigurable field-effect transistors, J. Phys.: Condens. Matter **31**, 355002 (2019).

[38] B. Müller, L. Hardt, A. Ambruster, K. Kiefer, and C. Reise, Yield predictions for photovoltaic power plants: Empirical validation, recent advances and remaining uncertainties, Prog. Photovolt: Res. Appl. **24**, 570 (2016).

[39] T. Kanne, M. Marnauza, D. Olsteins, D. J. Carrad, J. E. Sestoft, J. de Bruijckere, L. Zeng, E. Johnson, E. Olsson, K. Grove-Rasmussen, and J. Nygård, Epitaxial Pb on InAs nanowires for quantum devices, Nat. Nanotechnol. **16**, 776 (2021).

[40] C. R. H. McRae, J. H. Béjanin, C. T. Earnest, T. G. McConkey, J. R. Rinehart, C. Deimert, J. P. Thomas, Z. R. Wasilewski, and M. Mariantoni, Thin film metrology and microwave loss characterization of indium and aluminum/indium superconducting planar resonators, J. Appl. Phys. **123**, 205304 (2018).

[41] A. P. M. Place, L. V. H. Rodgers, P. Mundada, B. M. Smitham, M. Fitzpatrick, Z. Leng, A. Premkumar, J. Bryon, A. Vrajitoarea, S. Sussman, G. Cheng, T. Madhavan, H. K. Babla, X. H. Le, Y. Gang, B. Jäck, A. Gyenis, N. Yao, R. J. Cava, N. P. de Leon *et al.*, New material platform for superconducting transmon qubits with coherence times exceeding 0.3 milliseconds, Nat. Commun. **12**, 1779 (2021).

[42] I. I. Soloviev, S. V. Bakurskiy, V. I. Ruzhickiy, N. V. Klenov, M. Y. Kupriyanov, A. A. Golubov, O. V. Skryabina, and V. S. Stolyarov, Miniaturization of Josephson Junctions for Digital Superconducting Circuits, Phys. Rev. Applied **16**, 044060 (2021).

[43] W. D. Oliver and P. B. Welander, Materials in superconducting quantum bits, MRS Bull. **38**, 816 (2013).

[44] G. Kresse and J. Hafner, *Ab initio* molecular-dynamics simulation of the liquid-metal-amorphous-semiconductor transition in germanium, Phys. Rev. B **49**, 14251 (1994).

[45] G. Kresse and J. Furthmüller, Efficiency of *ab initio* total energy calculations for metals and semiconductors using a plane-wave basis set, Comput. Mater. Sci. **6**, 15 (1996).

[46] P. E. Blöchl, Projector augmented-wave method, Phys. Rev. B **50**, 17953 (1994).

[47] G. Kresse and D. Joubert, From ultrasoft pseudopotentials to the projector augmented-wave method, Phys. Rev. B **59**, 1758 (1999).

[48] L. G. Ferreira, M. Marques, and L. K. Teles, Approximation to density functional theory for the calculation of band gaps of semiconductors, Phys. Rev. B **78**, 125116 (2008).

[49] L. V. Bondarenko, A. Y. Tupchaya, A. N. Mihalyuk, S. V. Eremeev, A. V. Matetskiy, N. V. Denisov, Y. E. Vekovshinin, A. V. Slyshkin, D. V. Gruznev, A. V. Zotov, and A. A. Saranin, Fabrication and characterization of a single monolayer $NiSi_2$ sandwiched between Tl capping layer and a Si(111) substrate, 2D Mater. **7**, 025009 (2020).

[50] L. V. Bondarenko, A. Y. Tupchaya, Y. E. Vekovshinin, D. V. Gruznev, A. N. Mihalyuk, N. V. Denisov, A. V. Matetskiy, A. V. Zotov, and A. A. Saranin, $Pb/NiSi_2$ atomic sandwich on Si(111), Surf. Sci. **716**, 121966 (2022).

[51] S. S. Lee, H. J. Song, K. D. Kim, J. W. Chung, K. Kong, D. Ahn, H. Yi, B. D. Yu, and H. Tochihara, Structural and electronic properties of thallium overlayers on the Si(111)-7 × 7 surface, Phys. Rev. B **66**, 233312 (2002).

[52] N. D. Kim, C. G. Hwang, J. W. Chung, T. C. Kim, H. J. Kim, and D. Y. Noh, Structural properties of a thallium-induced Si(111)-1×1 surface, Phys. Rev. B **69**, 195311 (2004).

[53] See Supplemental Material at http://link.aps.org/supplemental/10.1103/PhysRevB.106.035415 for details on the (i) electronic band structures of $In/NiSi_2/Si(111)1 \times 1$ and $Tl/NiSi_2/Si(111)1 \times 1$ surfaces, and (ii) element-projected band structures of In-rect/Si(111) and In-rect/$NiSi_2$/Si(111) surfaces.

[54] E. Rotenberg, H. Koh, K. Rossnagel, H. W. Yeom, J. Schäfer, B. Krenzer, M. P. Rocha, and S. D. Kevan, Indium $\sqrt{7}\times\sqrt{3}$ on Si(111): A Nearly Free Electron Metal in Two Dimensions, Phys. Rev. Lett. **91**, 246404 (2003).

[55] S. Hikami, A. I. Larkin, and Y. Nagaoka, Spin-orbit interaction and magnetoresistance in the two dimensional random system, Prog. Theor. Phys. **63**, 707 (1980).

[56] A. A. Abrikosov, Magnetic impurities in nonmagnetic metals, Soviet Phys. Usp. **12**, 168 (1969).

[57] S. Yoshizawa, E. Minamitani, S. Vijayaraghavan, P. Mishra, Y. Takagi, T. Yokoyama, H. Oba, J. Niita, W. Sakamoto, T. Nakayama, and T. Uchihashi, Controlled modification of superconductivity in epitaxial atomic layer-organic molecule heterostructures, Nano Lett. **17**, 2287 (2017).

[58] A. Dahal, J. Gunasekera, L. Harringer, D. Singh, and D. Singh, Metallic nickel silicides: Experiments and theory for NiSi and first principles calculations for other phases, J. Alloys Compd. **672**, 110 (2016).

[59] S. Thirugnanasambandan, R. Thirugalathi Anbalagan, D. Saminathan, R. J. Joseyphus, N. Vengidusamy, and S. Arumainathan, Structure and magnetic properties of pulsed electrodeposited nickel-indium alloy, Phys. Status Solidi B **258**, 2000563 (2021).

[60] R. Bulla, T. A. Costi, and T. Pruschke, Numerical renormalization group method for quantum impurity systems, Rev. Mod. Phys. **80**, 395 (2008).

[61] P. Nozières, A "Fermi-liquid" description of the Kondo problem at low temperatures, J. Low Temp. Phys. **17**, 31 (1974).

[62] https://rscf.ru/project/19-12-00101/.

[63] https://cc.dvo.ru.